
Contracting Neural-Newton Solver

Samuel Chevalier, Jochen Stiasny, Spyros Chatzivasileiadis

Technical University of Denmark

Kgs. Lyngby, Denmark

{schev, jbest, spchatz}@elektro.dtu.dk

Abstract

Recent advances in deep learning have set the focus on neural networks (NNs) that can successfully replace traditional numerical solvers in many applications, achieving impressive computing gains. One such application is time domain simulation, which is indispensable for the design, analysis and operation of many engineering systems. Simulating dynamical systems with implicit Newton-based solvers is a computationally heavy task, as it requires the solution of a parameterized system of differential and algebraic equations at each time step. A variety of NN-based methodologies have been shown to successfully approximate the dynamical trajectories computed by numerical time domain solvers at a fraction of the time. However, so far no previous NN-based model has explicitly captured the fact that any predicted point on the time domain trajectory also represents the *fixed point* of the numerical solver itself. As we show, explicitly capturing this property can lead to significantly increased NN accuracy and much smaller NN sizes. In this paper, we model the Newton solver at the heart of an implicit Runge-Kutta integrator as a *contracting map* iteratively seeking this fixed point. Our primary contribution is to develop a recurrent NN simulation tool, termed the Contracting Neural-Newton Solver (CoNNS), which explicitly captures the contracting nature of these Newton iterations. To build CoNNS, we train a feedforward NN and mimic this contraction behavior by embedding a series of training constraints which guarantee the mapping provided by the NN satisfies the Banach fixed-point theorem; thus, we are able to prove that successive passes through the NN are guaranteed to converge to a unique, fixed point. Recent advances in NN training libraries (i.e., CVXPY Layers) allow us to embed our derived contraction constraints, which are posed as tractable semidefinite programs, directly into the NN training routine. We showcase the efficacy of the method through simulation results, gathered from a suite of engineering systems of varying dimensions. While CoNNS was developed for the specific application of time domain simulation, we conclude by showing that the underlying NN has the capacity to universally approximate any nonlinear system of equations which contract (e.g., Lyapunov functions, convex optimization solvers).

1 Introduction

Across many applications, Neural Networks (NNs) are being increasingly constructed, and subsequently utilized, as iterative self-mapping functions [7]:

$$\mathbf{x}^{(i+1)} = f(\mathbf{x}^{(i)}, \theta), \quad (1)$$

where the NN mapping $f : \mathbb{R}^n \rightarrow \mathbb{R}^n$ is parameterized by some input θ . Residual Networks (ResNets) [12], normalizing flows [18], and even standard Recurrent Neural Networks (RNNs) [55] all approximately leverage this self-mapping structure[7]. The observation that (1) can be interpreted as a forward Euler step [26, 11] of some underlying continuous dynamical system has lead to the

re-emergence [29, 9] of research which treats NNs as dynamical systems [22]. Notable recent works include, for example, Neural ODEs [7] with its many variants [29, 51, 41, 56], and Deep Equilibrium Models [2, 3]. These approaches, collectively referred to as Continuous Deep Learning Models (CDLMs), provide a variety of computational and modeling benefits, but they are also able to directly leverage a century worth of tools from the differential equations community.

The CDLM perspective arises by treating (1) as a discretized Euler step of some continuous system; in the limit, (1) transforms into a true derivative (i.e., $\dot{\mathbf{x}} = f(\mathbf{x}, \theta)$), and CDLMs naturally emerge [7]. In this paper, we offer a new perspective: rather than having (1) (or its continuous counterpart) directly model the evolution of some system of interest, we instead use it to model the iterative steps taken by the numerical *solver* of the system. In doing so, we can equip (1) with a particular mathematical property that few dynamical systems actually possess: contraction. Generally, a self-mapping system contracts if any input points are farther apart than the output points to which they map [40]. Thus, we use (1) to model a contracting numerical solver. As a guiding application, this paper focuses on modeling the expensive Newton solver which is at the computational heart of implicit Runge-Kutta integration [16]. If certain conditions are satisfied (e.g., conditions for the Newton-Kantorovich Theorem [36]), then Newton’s method is guaranteed to contract around the fixed point it is seeking. By ensuring that the Newton solver always iterates in a locally contracting region, we can train a NN which both mimics its contracting iterative behavior and, furthermore, is guaranteed to contract.

While emulating a Newton solver in the context of time domain simulation is our guiding application, the contributions from this paper help remove the barriers associated with using Machine Learning (ML) tools to replace conventional numerical solvers. The specific contributions of this work can be summarized as follows: (1) we derive conditions under which a NN of the form (1) is guaranteed to contract and thus satisfy the Banach fixed point theorem. (2) We pose these contraction conditions as simple, semidefinite programming constraints which can be implemented with open source tools (CVXPY Layers [1]) inside of the NN training routine. (3) We train the resulting NN, which we refer to as the Contracting Neural-Newton Solver (CoNNS), in order to mimic an actual contracting Newton solver. (4) We place CoNNS at the center of an implicit time domain simulation routine (trapezoidal method) in order to highlight its ability to replace a conventional Newton solver; test results are provided on three dynamical systems. (5) Finally, in order to show that the NN which underlays CoNNS can be used in applications beyond emulating a Newton solver, we prove that the associated NN can be used to universally approximate any self-mapping function which contracts. Modeling contracting systems while imposing the proposed constraints will lead to better, smaller ML models.

2 Related work

The direct modeling of dynamical systems using NNs has a rich history [10, 32, 19, 50]; subsequent simulation of the resulting parameterized models, though, requires the use of classical numerical solvers. Recently, attention has strongly shifted towards constructing models which are capable of *directly* predicting the time domain response of a dynamical system, thus bypassing the need for a numerical solver. In particular, the so-called Physics Informed Neural Network (PINN) [43], which uses physics-based sensitivities to regularize the training loss function, has achieved great success in extrapolating the solutions of Partial Differential Equations (PDE), both in continuous and discrete time applications. A variety of follow up works [38, 46, 25, 34] have quickly improved upon the method, adding additional training constraints and extending it into new domains. In particular, [45] formally extends PINN modeling to ODEs; ODE modeling will be the primary focus of this paper.

Rather than directly parameterizing a NN with an input time variable t , which is often necessary with PINNs, an alternative approximation scheme uses a *flow map* interpretation of dynamical systems [54]; in this case, a NN-based flow map function learns to directly advance a dynamical system state from $\mathbf{x}(t)$ to $\mathbf{x}(t + \Delta t)$. This is accomplished with a feedforward NN in [37] and a ResNet in [42]. The standard ResNet approach is improved upon in [24], where a hierarchy of ResNets is used in order overcomes the problem of numerical stiffness in dynamical systems. NNs which mimic flow maps, however, must implicitly model both the dynamics of a system and the application of a numerical integration tool [27] (e.g., implicit Runge-Kutta) all at once.

Ultimately, both PINNs and flow maps directly learn the trajectories associated with dynamical systems. Such trajectories, however, are always computed with numerical solvers. As explained in the Introduction, an even more fundamental approach to learning dynamical trajectories is to directly

learn the *iterative steps* taken by the associated numerical solver (assuming an implicit solver is used). Learning the behaviour of a numerical solver can be advantageous for a number of reasons, including the ability to model the evolution of a system with a smaller sized NN for a desired level of accuracy. While this approach has not been applied to the problem of time domain simulation, to the authors' knowledge, it has been applied in limited cases to other engineering problems [4, 30]. However, never has the convergence of the NN-based solver been explicitly addressed, much less guaranteed.

The convergence of our solver, CoNNs, simply coincides with the convergence of its RNN model. There is extensive work which analyzes the stability of RNNs, beginning with [47]. Textbook [53] offers comprehensive theoretical convergence analysis of RNNs; however, discrete RNNs (which are the focus of this paper) are only analyzed in the context of energy functions, and the resulting analytical conditions for stability are intractable for large, deep NNs. Other rigorous energy function formulations are offered in [6, 35, 15]. More recently, [8] enforced stability of discrete RNNs by conservatively constraining eigenvalues of weighting matrices via Gershgorin circle theorem.

In this paper, we target contraction, which is a stronger notion than stability, but has sparsely been addressed in the discrete RNN literature until very recently. [48] was one of the first papers which derived sufficient conditions for the contraction of a single layer RNN with bounded activation functions. Subsequently, [28] developed analytical conditions related to the slope of the sigmoid activation function and the size of the weighting parameters, again for a single layer NN. Most recently, [33] investigated the stability of RNNs from the perspective of so-called λ -contractive sets (see [5]) for the application of language prediction. These methods are improved upon and analyzed in [44], where projected gradient descent is used to project the NN model into a contracting space. In both [33] and [44], however, contraction of the RNN is utilized only as a conservative proxy to achieve stability; in neither case is convergence to a unique fixed point an explicit goal (or even a consideration) for the underlying RNN. In this work, we embed contraction conditions since the system we are modeling truly does contract.

3 Mathematical background

3.1 Useful matrix properties

In this paper, we denote $\rho(\cdot)$ as the spectral radius operator, i.e., $\rho(\mathbf{A}) \triangleq \max\{|\lambda(\mathbf{A})|\}$, $\mathbf{A} \in \mathbb{R}^{n \times n}$, and we denote $\varsigma_m(\cdot)$ as the maximum singular value operator, i.e., $\varsigma_m(\mathbf{A}) = \max\{\sqrt{\lambda(\mathbf{A}\mathbf{A}^T)}\}$ [13]. We reserve the operator $\sigma(\cdot)$ (which often denotes singular values) for the standard ReLU function. Notably, the largest singular value of a matrix upper bounds the spectral radius via $\rho(\mathbf{A}) \leq \varsigma_m(\mathbf{A})$, with strict equality when \mathbf{A} is symmetric. The largest singular value bounds the norm of transformed vector \mathbf{x} via $\|\mathbf{A}\mathbf{x}\|_2 \leq \varsigma_m(\mathbf{A})\|\mathbf{x}\|_2$; this bound holds for the spectral radius when $\mathbf{A} = \mathbf{A}^T$.

3.2 Fixed points of contracting systems

Definition 1 (Contraction Mapping [40]). *A function $\mathbf{f} : \mathbb{R}^n \rightarrow \mathbb{R}^n$ is said to be **contracting**, or equivalently, a **contraction mapping**, on \mathbb{R}^n if, for any $\mathbf{x}, \mathbf{y} \in \mathbb{R}^n$, there exists $0 \leq \mu < 1$ such that*

$$\|\mathbf{f}(\mathbf{x}) - \mathbf{f}(\mathbf{y})\|_2 \leq \mu \|\mathbf{x} - \mathbf{y}\|_2. \quad (2)$$

Using this definition of contraction,¹ we recall the celebrated Banach Fixed-Point Theorem (FPT).

Theorem 1 (Banach Fixed-Point Theorem [40]). *Let $\mathbf{f} : \mathbb{R}^n \rightarrow \mathbb{R}^n$ be contracting on the complete metric space of \mathbb{R}^n . Then, \mathbf{f} has a unique fixed point \mathbf{x}^* , such that $\mathbf{x}^* = \mathbf{f}(\mathbf{x}^*)$. Moreover, for any $\mathbf{x} \in \mathbb{R}^n$, the sequence $\mathbf{f} \circ \cdots \circ \mathbf{f} \circ \mathbf{f}(\mathbf{x})$ converges to \mathbf{x}^* .*

3.3 Implicit Runge-Kutta Integration

We consider a time-invariant system of nonlinear Ordinary Differential Equations (ODEs) given as

$$\dot{\mathbf{x}}(t) \triangleq \frac{d}{dt} \mathbf{x}(t) = \mathbf{f}(\mathbf{x}(t)). \quad (3)$$

¹Contraction mappings are often defined with respect to some metric space \mathcal{X} equipped with a suitable distance operator $d(\cdot)$. In our application, however, we target the specific metric space of \mathbb{R}^n equipped with the Euclidean distance metric (i.e., the l_2 norm $\|\cdot\|_2$).

The goal of time domain simulation [24] is to integrate (3) forward in time via

$$\mathbf{x}(t + \Delta t) = \mathbf{x}(t) + \int_t^{t + \Delta t} \mathbf{f}(\mathbf{x}(\tau)) d\tau. \quad (4)$$

Since the closed form solution of (4) is rarely available, (3) is typically integrated using a Runge-Kutta time-stepping approach. Depending on how the parameters of the integration scheme are chosen, Runge-Kutta methods can take the form of many popular integrators (e.g., backward Euler); these methods can be classified as either explicit or implicit. In this work, we exclusively consider implicit integration schemes, since they are the overwhelming choice for many physics-based applications, yet they are computationally expensive to solve. In the Implicit Runge-Kutta (IRK) method [16], the future state $\mathbf{x}(t + \Delta t)$ is written as the sum

$$\mathbf{x}(t + \Delta t) = \mathbf{x}(t) + \Delta t \sum_{i=1}^s b_i \mathbf{k}_i, \quad (5)$$

where s is the number of “stages” associated with the IRK method, and \mathbf{k}_i is a vector of trajectory derivatives at various points $t + c_i \Delta t$ between t and $t + \Delta t$. These derivative terms are computed as

$$\mathbf{k}_i = \mathbf{f} \left(\mathbf{x}(t) + \Delta t \sum_{j=1}^s \alpha_{i,j} \mathbf{k}_j \right), \quad i \in \{1, \dots, s\}. \quad (6)$$

The parameters $\alpha_{i,j}$, b_i , and c_i are given coefficients from the Butcher tableau. Notably, the Runge-Kutta step given by (5)-(6) represents an implicit, nonlinear system of equations. Typically, an iterative root finding tool, such as Newton’s method, is used to drive this system of nonlinear equations to $\mathbf{0}$ at each time step. Without loss of generality, this paper will focus exclusively on the trapezoidal integration (TI) method [16] as a guiding example, since TI is the primary workhorse behind many ODE solvers [31]. With TI, the implicit system of equations associated with (6) is given by

$$\mathbf{0} = \mathbf{k}_2 - \mathbf{f}(\mathbf{x}(t) + \frac{\Delta t}{2} \mathbf{k}_1 + \frac{\Delta t}{2} \mathbf{k}_2) \triangleq \mathbf{K}_t(\mathbf{k}_2), \quad (7)$$

where $\mathbf{k}_1 = \mathbf{f}(\mathbf{x}(t))$. System (7) is typically solved by linearizing $\mathbf{K}_t(\mathbf{k}_2) \approx \mathbf{K}_t(\mathbf{k}_2^{(0)}) + \mathbf{J}_t(\mathbf{k}_2^{(0)}) \Delta \mathbf{k}_2$, setting the expression equal to $\mathbf{0}$, and then defining the iterative self-map

$$\mathbf{k}_2^{(i+1)} = \underbrace{\mathbf{k}_2^{(i)} - \mathbf{J}_t(\mathbf{k}_2^{(i)})^{-1} \mathbf{K}_t(\mathbf{k}_2^{(i)})}_{\mathbf{G}(\mathbf{k}_2^{(i)})}. \quad (8)$$

The primary computational bottleneck associated with IRK integration comes from the time needed to solve nonlinear system (7) by iterating on (8).

4 The Contracting Neural-Newton Solver (CoNNS)

In this section, we build a NN which effectively emulates the Newton solver routine in (8). To do so, we train a standard feedforward NN on the actual Newton steps taken by a Newton solver, but we apply a series of training constraints to ensure contraction of the NN mapping.

4.1 Newton iterations as a contraction mapping

In constructing the Contracting Neural-Newton Solver (CoNNS), we begin by casting the Newton iterations from (8) as a contracting system which is searching for a fixed point. Generally, \mathbf{G} may not contract for an arbitrarily large time step Δt or arbitrarily chosen initial conditions. However, in this work, we assume these values are chosen such that \mathbf{G} does represent a contracting system. Contraction in some region can be guaranteed by applying conditions from the Newton-Kantorovich Theorem [36] or by ensuring the system’s Lipschitz constant is less than 1. An even simpler condition bounds the gradient of the function over some convex set \mathcal{X} to be less than 1: $f'(x) < 1, \forall x \in \mathcal{X}$ in the scalar case. We may define analogous conditions in n -dimensions. Setting $\mathbf{K} \triangleq \mathbf{K}_t(\mathbf{k}_2)$ and $\mathbf{J} \triangleq \mathbf{J}_t(\mathbf{k}_2)$, the following sufficient condition ensures (8) will contract over convex set \mathcal{K} :

$$\varsigma_m \left(\mathbf{J}^{-1} \left[\begin{array}{cccc} (\frac{\partial}{\partial \mathbf{k}_{21}} \mathbf{J}) \mathbf{J}^{-1} \mathbf{K} & (\frac{\partial}{\partial \mathbf{k}_{22}} \mathbf{J}) \mathbf{J}^{-1} \mathbf{K} & \cdots & (\frac{\partial}{\partial \mathbf{k}_{2n}} \mathbf{J}) \mathbf{J}^{-1} \mathbf{K} \end{array} \right] \right) < 1, \quad \forall \mathbf{k}_2 \in \mathcal{K}. \quad (9)$$

Assumption 1. When solving nonlinear system (7) via (8), the time step size Δt and initialization of \mathbf{k}_2 are always chosen a priori to ensure that (9) is satisfied and, therefore, (8) contracts.

The derivation of (9) can be found in the Appendix. Assumption 1 often holds in practice for suitably small time steps. When it does not hold, the size of the time step Δt can always be lowered.

4.2 Conditions for guaranteed contraction of a neural network

Inspired by the contracting behaviour of (8), we now seek to train a feedforward NN $\Phi : \mathbb{R}^{2n} \rightarrow \mathbb{R}^n$ which mimics a Newton solver and is additionally guaranteed to have contraction characteristics. Thus, each pass through the NN will analogously represent a single iteration of the Newton solver; repeated passes will converge to a fixed point. We define an h -layer NN $\mathbf{k}_2^{(i+1)} = \Phi(\mathbf{k}_2^{(i)}, \mathbf{x}(t))$ via

$$\mathbf{k}_2^{(i+1)} = \underbrace{\sigma \left(\mathbf{W}_h \dots \sigma \left(\mathbf{W}_2 \sigma \left(\mathbf{W}_1 \mathbf{k}_2^{(i)} + \mathbf{U} \mathbf{x}(t) + \mathbf{b}_1 \right) + \mathbf{b}_2 \right) \dots + \mathbf{b}_h \right)}_{\Phi(\mathbf{k}_2^{(i)}, \mathbf{x}(t))} \quad (10)$$

where $\sigma(\cdot)$ is the ReLU function. Notably, the NN is parameterized by two inputs: $\mathbf{k}_2^{(i)} \in \mathbb{R}^n$, which is updated during each iteration of (10), and $\mathbf{x}(t) \in \mathbb{R}^n$, which is invariant during each iteration of (10). The weighting matrices in (10) have dimensions $\mathbf{U}, \mathbf{W}_1 \in \mathbb{R}^{m \times n}$, $\mathbf{W}_h \in \mathbb{R}^{n \times m}$, and $\mathbf{W}_i \in \mathbb{R}^{m \times m}$, $i \in \{2, \dots, h-1\}$, where generally $m \gg n$. In the sequel, we present a series of conditions which are necessary to ensure the self-mapping routine (10) will contract.

Lemma 1. For all vectors $\mathbf{x}, \mathbf{y} \in \mathbb{R}^n$, the ReLU operator $\sigma : \mathbb{R}^n \rightarrow \mathbb{R}^n$ satisfies

$$\|\sigma(\mathbf{x}) - \sigma(\mathbf{y})\|_p \leq \|\mathbf{x} - \mathbf{y}\|_p, \quad \forall p \in \{1, 2, \dots, \infty\}. \quad (11)$$

Proof. In the scalar case, $|\sigma(x) - \sigma(y)| \leq |x - y|$. Applying the p -norm definition [13],

$$\|\mathbf{x} - \mathbf{y}\|_p = \left(\sum_{i=1}^n |\mathbf{x}_i - \mathbf{y}_i|^p \right)^{1/p} \leq \left(\sum_{i=1}^n |\sigma(\mathbf{x}_i) - \sigma(\mathbf{y}_i)|^p \right)^{1/p} = \|\sigma(\mathbf{x}) - \sigma(\mathbf{y})\|_p. \quad \square$$

We now consider a single i^{th} layer of (10):

$$\mathbf{x} = \sigma(\mathbf{W}_i \mathbf{x} + \mathbf{b}_i) \triangleq \mathbf{g}(\mathbf{x}). \quad (12)$$

Lemma 2. If $\varsigma_m(\mathbf{W}_i) < 1$, then (12) is a contraction mapping.

Proof. We directly apply the definition of contraction (2) for arbitrary inputs \mathbf{x} and \mathbf{y} :

$$\|\mathbf{g}(\mathbf{x}) - \mathbf{g}(\mathbf{y})\|_2 = \|\sigma(\mathbf{W}_i \mathbf{x} + \mathbf{b}_i) - \sigma(\mathbf{W}_i \mathbf{y} + \mathbf{b}_i)\|_2 \quad (13a)$$

$$= \|\sigma(\hat{\mathbf{x}}) - \sigma(\hat{\mathbf{y}})\|_2 \quad (13b)$$

$$\leq \|\hat{\mathbf{x}} - \hat{\mathbf{y}}\|_2 \quad (13c)$$

$$= \|\mathbf{W}_i(\mathbf{x} - \mathbf{y}) + \mathbf{b}_i - \mathbf{b}_i\|_2 \quad (13d)$$

$$\leq \varsigma_m(\mathbf{W}_i) \|\mathbf{x} - \mathbf{y}\|_2, \quad (13e)$$

where (13c) is justified by (11). Since $\varsigma_m(\mathbf{W}_i) < 1$, (2) is satisfied and (12) necessarily contracts. \square

Lemma 2 may be used to derive a sufficient condition to ensure (10) satisfies the Banach FPT.

Theorem 2. Assume the h -layer NN $\mathbf{k}_2 = \Phi(\mathbf{k}_2, \mathbf{x}(t))$ of (10) satisfies

$$\sup_{i \in \{1, \dots, h\}} \varsigma_m(\mathbf{W}_i) < 1. \quad (14)$$

This is a sufficient condition to ensure that (10) satisfies the Banach Fixed-Point Theorem.

Proof of Theorem 2. Write (10) as a sequence of mappings:

$$\mathbf{g}_1(\mathbf{k}_2) = \sigma(\mathbf{W}_1 \mathbf{k}_2 + \mathbf{U} \mathbf{x}(t) + \mathbf{b}_1) \quad (15)$$

$$\mathbf{g}_2(\mathbf{k}_2) = \sigma(\mathbf{W}_2 \mathbf{g}_1(\mathbf{k}_2) + \mathbf{b}_2) \quad (16)$$

⋮

$$\mathbf{g}_h(\mathbf{k}_2) = \sigma(\mathbf{W}_h \mathbf{g}_{h-1}(\mathbf{k}_2) + \mathbf{b}_h). \quad (17)$$

By Lemma 2, each of these functions represents a contraction if (14) is satisfied. The composition of functions $\Phi \triangleq g_n \circ \dots \circ g_2 \circ g_1$ which are individually contracting results in a new function which is also contracting. Thus, $\Phi(\mathbf{k}_2, \mathbf{x}(t))$ is contracting and necessarily satisfies the Banach FPT. \square

Directly constraining the singular values of a matrix (i.e., via (14)) in a NN training environment is challenging. Instead, we seek to use semidefinite programming (SDP) tools which can efficiently constrain matrix eigenvalues. Furthermore, such tools are conveniently available through emerging toolboxes (i.e., CVXPY Layers [1]) which integrate seamlessly into popular training environments. Accordingly, we define two tractable alternatives for ensuring (14) is satisfied using SDP tools.

Enforcing Symmetry: As noted, $\rho(\mathbf{W}) = \varsigma_m(\mathbf{W})$ when $\mathbf{W} = \mathbf{W}^T$. Accordingly, if the addition (subtraction) of an identity matrix maps $\mathbf{W} = \mathbf{W}^T$ to a positive (negative) definite space, then the maximum singular value of the original matrix is guaranteed to be less than unity. Since SDP programming tools only allow for semidefinite, rather than definite, constraints, we introduce a small factor, ϵ , where $0 < \epsilon \ll 1$, in order to slightly scale down the identity matrix. Therefore,

$$\left. \begin{array}{l} \mathbf{W} = \mathbf{W}^T \\ \mathbf{W} - \mathbf{I}(1 - \epsilon) \preceq \mathbf{0} \\ \mathbf{W} + \mathbf{I}(1 - \epsilon) \succeq \mathbf{0} \end{array} \right\} \Rightarrow \varsigma_m(\mathbf{W}) < 1. \quad (18)$$

Schur Complement: While (18) is a simple condition, the symmetry constraint might be undesirable, or overly restrictive, in certain applications. To remove this symmetry condition, at the cost of computational expense, we note that $\sigma(\mathbf{W}) < 1$ implies $\lambda(\mathbf{W}\mathbf{W}^T) < 1$, and furthermore, $\mathbf{I} - \mathbf{W}\mathbf{I}^{-1}\mathbf{W}^T \succ \mathbf{0}$, as in [52]. By the Schur complement lemma [52, 44]

$$\left[\begin{array}{cc} \mathbf{I}(1 - \epsilon) & \mathbf{W} \\ \mathbf{W}^T & \mathbf{I}(1 - \epsilon) \end{array} \right] \succeq \mathbf{0} \Rightarrow \varsigma_m(\mathbf{W}) < 1, \quad (19)$$

which introduces a very small, i.e., $\mathcal{O}(\epsilon)$, degree of conservativeness. While (19) is a generally less restrictive (because there is no symmetry constraint), (18) is computationally cheaper to implement.

Remark 1. *The contraction condition (14) in Theorem 2 can be satisfied for all square matrices by imposing either (18) or (19) using conventional SDP tools.*

While matrices in all hidden layers of (10) are assumed square, the input and output matrices \mathbf{W}_1 and \mathbf{W}_h are generally non-square. To overcome the complication on non-square matrices, we define square, augmented matrices $\tilde{\mathbf{W}}_1 = [\mathbf{W}_1 \mid \mathbf{M}_1] \in \mathbb{R}^{n \times n}$ and $\tilde{\mathbf{W}}_h = [\mathbf{W}_h^T \mid \mathbf{M}_h^T]^T \in \mathbb{R}^{n \times n}$.

Remark 2. *If $\tilde{\mathbf{W}}_1$ (resp., $\tilde{\mathbf{W}}_h$) satisfies (18) or (19), then $\varsigma_m(\mathbf{W}_1) < 1$ (resp., $\varsigma_m(\mathbf{W}_h) < 1$).*

4.3 Constrained training procedure

In order to teach a NN the contracting characteristics of a Newton solver, (10) is explicitly trained on Newton step data. Using CVXPY Layers [1], however, we define a convex SDP which, at each training step, optimally projects the unconstrained matrix \mathbf{W}_i into a constrained space via

$$\begin{aligned} \min_{\hat{\mathbf{W}}_i} \quad & \|\mathbf{W}_i - \hat{\mathbf{W}}_i\|_F^2 \\ \text{s.t.} \quad & (18) \text{ or } (19), \end{aligned} \quad (20)$$

$\forall i \in \{2, \dots, h-1\}$. Once solved, the value of \mathbf{W}_i is updated via $\mathbf{W}_i \leftarrow \hat{\mathbf{W}}_i$. For non-square matrices \mathbf{W}_1 and \mathbf{W}_h , formulation (20) is updated such that the SDP minimizes the difference between a non-square matrix and its constrained counterpart; the augmented version of the decision matrix is constrained via (18) or (19). For example, to constrain \mathbf{W}_1 via (19), we define

$$\begin{aligned} \min_{\hat{\mathbf{W}}_1, \mathbf{M}_1} \quad & \|\mathbf{W}_1 - \hat{\mathbf{W}}_1\|_F^2 \\ \text{s.t.} \quad & \left[\begin{array}{cc} \mathbf{I}(1 - \epsilon) & [\hat{\mathbf{W}}_1 \mid \mathbf{M}_1] \\ [\hat{\mathbf{W}}_1 \mid \mathbf{M}_1] & \mathbf{I}(1 - \epsilon) \end{array} \right] \succeq \mathbf{0}. \end{aligned} \quad (21)$$

A similar (but transposed) formulation can be stated for output matrix \mathbf{W}_h . After every training step, projections (20) and (21) guarantee the NN will always satisfy the Banach FPT.

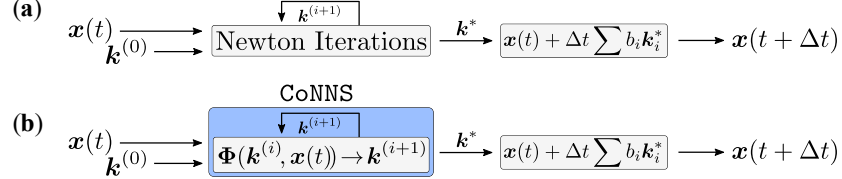


Figure 1: Diagram (a) shows the conventional computational flow associated with IRK integration. In diagram (b), the expensive Newton solver is replaced by CoNNS.

Convergence of this constrained training routine is greatly aided by properly initializing the NN weight matrices. In the Appendix, we develop a procedure which uses QR decomposition of sampled training data after an unconstrained train in order to produce a useful initialization.

4.4 Embedding CoNNS inside time domain integration

In Fig. 1, we portray the intended use of CoNNS in the context of time domain simulation: it replaces the expensive Newton solver at the heart of IRK integration with recurrent calls of the contracting NN Φ . As CoNNS iterates, it is guaranteed to find some fixed point \mathbf{k}^* ; this point is then used to predict the next time step $\mathbf{x}(t + \Delta t)$. In the case of trapezoidal integration, $\mathbf{x}(t + \Delta t) = \mathbf{x}(t) + \frac{1}{2}\mathbf{f}(\mathbf{x}(t)) + \frac{1}{2}\mathbf{k}_2^*$. Of course, while this \mathbf{k}_2^* will represent the fixed point of the NN, it may not be the exact fixed point of the actual Newton solver; the quality of this prediction is a function of how well the NN was trained.

5 Numerical test results

In this section, we provide test results associated with three simulated systems: a two-state cubic oscillator [24], a three-state Hopf bifurcation [24], and a 10-state electrical power system, known as the two-area Kundur system [20], which represents a network of nonlinear coupled oscillators.

Cubic Oscillator:	Hopf bifurcation:	Kundur system:
$\dot{x} = -0.1x^3 + 2y^3$	$\dot{\mu} = 0$	$\dot{\delta}_i = \omega_i$
$\dot{y} = -2x^3 - 0.1y^3$	$\dot{x} = \mu x + y - x(x^2 + y^2)$	$\dot{\omega}_i = \hat{p}_i - \hat{d}_i \omega_i - \sum \hat{B}_{ij} \sin(\delta_i - \delta_j)$
	$\dot{y} = \mu y - x - y(x^2 + y^2)$	$\forall i \in \mathcal{I}$

To collect training data, we defined a set of initial conditions associated with each system, and we randomly perturbed these conditions in order to generate a strong system perturbation. We then simulated the resulting deterministic trajectories, for between 3 and 45 seconds, via the standard integration method presented in panel (a) of Fig. 1. In doing so, we used a step size Δt between 0.025s and 0.001s, and we employed trapezoidal integration; tolerance for Newton convergence was set to $\epsilon = 10^{-9}$. Additional settings can be found directly in the code.

After collecting between 40 and 50 time domain trajectories for each system, we trained CoNNS directly on the Newton step data, as parameterized by the location in state space $\mathbf{x}(t)$ (see (10)). Training was performed with PyTorch [39] (BSD license), and we used CVXPY Layers [1] (Apache 2.0 license) in order to implement the derived constraints by solving (20) using (19). In order to train the networks, we used the Adam optimizer [17], with learning rates set between 10^{-4} and 10^{-5} . No data batching was performed; all simulation and training was performed on a Dell XPS laptop equipped with an Intel i7 CPU @ 2.60GHz 16 GB of RAM. We trained NNs containing three hidden layers with 40 and 50 nodes per layer for the cubic oscillator and Hopf bifurcation systems, respectively. The NN for the Kundur system contained 100 nodes per hidden layer; see the Appendix for details. In each case, all layers except for the final one contained ReLU activation functions; the last layer contained a linear activation function, since \mathbf{k}_2 is unconstrained.

We evaluate the performance of the resulting CoNNS by testing it on 50 trajectories stemming from the same distribution as the training set. We bench-marked against an equivalently sized NN which was trained with no contraction constraints; both networks were trained to the same level of loss. Table 1 reports the results on the training and test set for the cubic oscillator, both in the constrained and unconstrained versions. The $\|\cdot\|_2$ norm evaluates the error between the predicted states \hat{x}, \hat{y} and the ground-truth states x, y across a single trajectory, as shown in Fig. 2. In the rows of Table 1 we give

Table 1: Training and test error, computed as the mean, standard deviation, and maximum value of the 2-norm on the approximation error across a trajectory. The number of iterations is the cumulative count of passes through CoNNS or the unconstrained NN for a given trajectory (Newton required a maximum of 8950 iterations, for reference).

Metric	Data	Cubic oscillator (constrained)			Cubic oscillator (unconstrained)		
		$\ x - \hat{x}\ _2$	$\ y - \hat{y}\ _2$	iterations	$\ x - \hat{x}\ _2$	$\ y - \hat{y}\ _2$	iterations
mean	Training	0.3685	0.3620	12873	7.8412	7.9659	216531
sd	Training	0.3394	0.3442	1675	4.3590	4.5314	14528
max	Training	1.4939	1.4683	16044	16.7858	18.1205	236942
mean	Test	0.7297	0.7279	13177	8.7604	8.8905	213619
sd	Test	0.8200	0.8230	1728	5.4595	5.2871	21309
max	Test	4.0938	4.2462	16413	21.9004	22.5338	237974

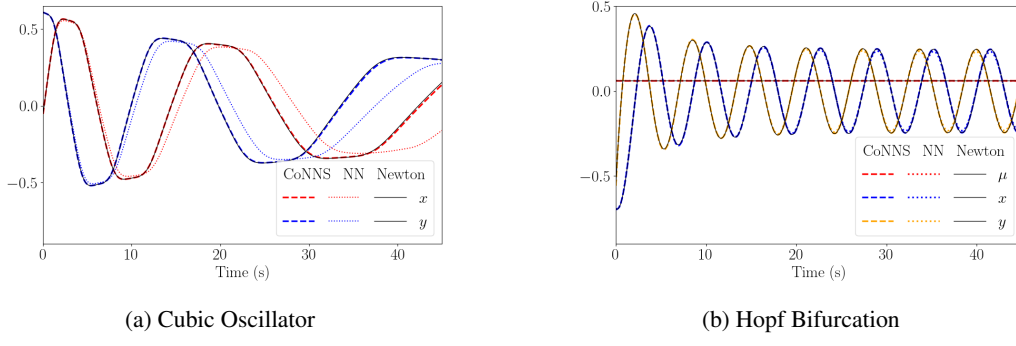


Figure 2: System trajectories simulated with Newton, CoNNS and an unconstrained NN.

summary statistics across the 50 evaluated trajectories. Detailed results for the other systems can be found in the Appendix. The results suggest a much more reliable prediction with CoNNS as compared to the unconstrained network; furthermore, CoNNS required notably fewer iterations to reach fixed point convergence. The vector fields and the distribution of the singular values are shown in Fig. 3. The vector fields associated with the two networks differ significantly around the fixed point (blue), affecting the required number of iterations. We further note, that for the cubic oscillator and Hopf bifurcation systems, we are able to achieve a level of accuracy with CoNNS that is equivalent to recent results reported in [23]; however, the size of our NNs is approximately $3 \times$ smaller.

5.1 Discussion: computational complexity of CoNNS and methodological limitations

For a dynamical system with p states, the computational complexity of a single iteration of Newton’s method is dominated by the linear system solve $\mathbf{J}^{-1}\mathbf{K}$, which is $\mathcal{O}(p^3)$, assuming the Jacobian function is available apriori. If the CoNNS NN is h layers deep with m nodes per layer, evaluation of the network will require h matrix-vector products, for a total cost of $\mathcal{O}(h \cdot m^2)$. Since $m \gg h$, though, the cost is closer to $\sim \mathcal{O}(m^2)$. Because CoNNS and Newton require a similar number of iterations to converge (at least, same order of magnitude), CoNNS will begin to offer computational benefits only when $p^{3/2} > m$. Thus, CoNNS will offer its primarily computational advantages in large systems, especially ones which evolve in low dimensional subspaces. One of the main limitations of CoNNS, however, comes from the computational cost of training with the SDP constraints, e.g., (19). For matrices that are $\mathbb{R}^{100 \times 100}$, iterative Adam steps slow down by almost an order of magnitude.

6 CoNNS as a universal approximator of contracting functions

Feedforward NNs possess the powerful trait of universal approximation [14, 21]. While CoNNS emulates a Newton solver, we note that the underlying neural network (e.g., (10), subject to (19)) can universally approximate any self-mapping function which contracts (see Appendix for proof).

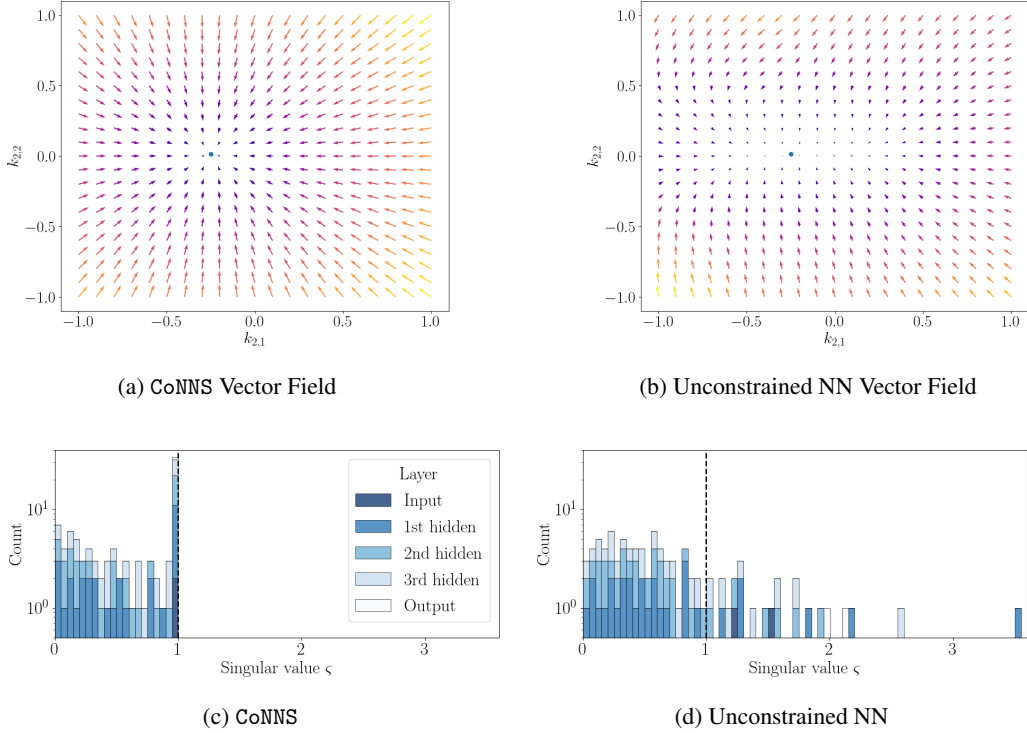


Figure 3: The top panels show vector fields of $\Phi(\mathbf{k}_2, \mathbf{x}(t))$ for the cubic oscillator; arrows represent $\mathbf{k}_2^{(i+1)} - \Phi(\mathbf{k}_2^{(i)}, \mathbf{x}(t))$ with $\mathbf{k}_2 = [k_{2,1}, k_{2,2}]^T$ for $\mathbf{x}(t) = [-0.1, -0.5]^T$ for CoNNS (a) and an unconstrained NN (b). Panels (c), (d) show the singular values of the weight matrices, color coded according to the layer (the count is displayed on a logarithmic scale). Clearly, singular values of the CoNNS system are all bounded by 1, guaranteeing contraction.

Theorem 3. *A self-mapping, feedforward NN of the form (1) equipped with ReLU activation functions and whose weighting matrices satisfy (14) is a universal approximator of any contracting function.*

As a direct corollary, our training methodology can be employed to enforce (14) without sacrificing universal approximation. This highlights the generality of our approach, and it indicates our methodology can be useful for modeling a variety of contracting functions across many fields.

7 Conclusion

In order to model a contracting numerical solver, this paper developed a set of conditions which, when imposed, guarantee a self-mapping NN will also contract and thus satisfy the Banach FPT. Using this framework, we built a Contracting Neural-Newton Solver (CoNNS) for the purpose of accelerating implicit Runge-Kutta time domain integration. From our test results, we can conclude that the training constraints (i) help improve the accuracy of the trained model, as compared to the accuracy of the unconstrained model, and (ii) help reduce the size of the model, for a given level of desired accuracy. Future work will focus on modeling other contracting systems, and it will seek to test our modeling strategy on larger systems of equations. Through this work, we seek to remove the barriers associated with using ML to emulate numerical solvers, and we therefore envision a variety of positive societal impacts (e.g., faster contingency screenings in safety critical applications). However, faster numerical solvers could be exploited by a variety of institutions (e.g., non-sustainable industries) in order to enhance the efficiency of their engineering systems.

References

- [1] Akshay Agrawal, Brandon Amos, Shane Barratt, Stephen Boyd, Steven Diamond, and J. Zico Kolter. Differentiable convex optimization layers. In H. Wallach, H. Larochelle, A. Beygelzimer, F. d’Alché-Buc, E. Fox, and R. Garnett, editors, *Advances in Neural Information Processing Systems*, volume 32. Curran Associates, Inc., 2019. URL <https://proceedings.neurips.cc/paper/2019/file/9ce3c52fc54362e22053399d3181c638-Paper.pdf>.
- [2] Shaojie Bai, J Zico Kolter, and Vladlen Koltun. Deep equilibrium models. *arXiv preprint arXiv:1909.01377*, 2019.
- [3] Shaojie Bai, Vladlen Koltun, and J Zico Kolter. Multiscale deep equilibrium models. *arXiv preprint arXiv:2006.08656*, 2020.
- [4] Kyri Baker. Emulating ac opf solvers for obtaining sub-second feasible, near-optimal solutions. *arXiv preprint arXiv:2012.10031*, 2020.
- [5] Franco Blanchini and Stefano Miani. *Set-theoretic methods in control*. Springer, 2008.
- [6] Jinde Cao and Jun Wang. Global asymptotic and robust stability of recurrent neural networks with time delays. *IEEE Transactions on Circuits and Systems I: Regular Papers*, 52(2):417–426, 2005. doi: 10.1109/TCSI.2004.841574.
- [7] Ricky TQ Chen, Yulia Rubanova, Jesse Bettencourt, and David Duvenaud. Neural ordinary differential equations. *arXiv preprint arXiv:1806.07366*, 2018.
- [8] Marco Ciccone, Marco Gallieri, Jonathan Masci, Christian Osendorfer, and Faustino Gomez. NAIS-Net: Stable Deep Networks from Non-Autonomous Differential Equations. *arXiv e-prints*, art. arXiv:1804.07209, April 2018.
- [9] Michael A. Cohen and Stephen Grossberg. Absolute stability of global pattern formation and parallel memory storage by competitive neural networks. *IEEE Transactions on Systems, Man, and Cybernetics*, SMC-13(5):815–826, 1983. doi: 10.1109/TSMC.1983.6313075.
- [10] R. González-García, R. Rico-Martínez, and I.G. Kevrekidis. Identification of distributed parameter systems: A neural net based approach. *Computers & Chemical Engineering*, 22: S965–S968, 1998. ISSN 0098-1354. doi: [https://doi.org/10.1016/S0098-1354\(98\)00191-4](https://doi.org/10.1016/S0098-1354(98)00191-4). URL <https://www.sciencedirect.com/science/article/pii/S0098135498001914>. European Symposium on Computer Aided Process Engineering-8.
- [11] Eldad Haber and Lars Ruthotto. Stable architectures for deep neural networks. *Inverse Problems*, 34(1):014004, 2017.
- [12] Kaiming He, Xiangyu Zhang, Shaoqing Ren, and Jian Sun. Deep residual learning for image recognition. In *2016 IEEE Conference on Computer Vision and Pattern Recognition (CVPR)*, pages 770–778, 2016. doi: 10.1109/CVPR.2016.90.
- [13] R.A. Horn and C.R. Johnson. *Matrix Analysis*. Cambridge University Press, 1990. ISBN 9780521386326.
- [14] Kurt Hornik, Maxwell Stinchcombe, and Halbert White. Multilayer feedforward networks are universal approximators. *Neural Networks*, 2(5):359–366, 1989. ISSN 0893-6080. doi: [https://doi.org/10.1016/0893-6080\(89\)90020-8](https://doi.org/10.1016/0893-6080(89)90020-8). URL <https://www.sciencedirect.com/science/article/pii/0893608089900208>.
- [15] Sanqing Hu and Jun Wang. Global stability of a class of discrete-time recurrent neural networks. *IEEE Transactions on Circuits and Systems I: Fundamental Theory and Applications*, 49(8): 1104–1117, 2002. doi: 10.1109/TCSI.2002.801284.
- [16] Arieh Iserles. *A First Course in the Numerical Analysis of Differential Equations*. Cambridge Texts in Applied Mathematics. Cambridge University Press, 2 edition, 2008. doi: 10.1017/CBO9780511995569.
- [17] Diederik P Kingma and Jimmy Ba. Adam: A method for stochastic optimization. *arXiv preprint arXiv:1412.6980*, 2014.

[18] Ivan Kobyzev, Simon Prince, and Marcus Brubaker. Normalizing flows: An introduction and review of current methods. *IEEE Transactions on Pattern Analysis and Machine Intelligence*, 2020.

[19] E.B. Kosmatopoulos, M.M. Polycarpou, M.A. Christodoulou, and P.A. Ioannou. High-order neural network structures for identification of dynamical systems. *IEEE Transactions on Neural Networks*, 6(2):422–431, 1995. doi: 10.1109/72.363477.

[20] Prabha Kundur et al. *Power system stability and control*, volume 7. McGraw-Hill New York, 1994.

[21] Moshe Leshno, Vladimir Ya. Lin, Allan Pinkus, and Shimon Schocken. Multilayer feed-forward networks with a nonpolynomial activation function can approximate any function. *Neural Networks*, 6(6):861–867, 1993. ISSN 0893-6080. doi: [https://doi.org/10.1016/S0893-6080\(05\)80131-5](https://doi.org/10.1016/S0893-6080(05)80131-5). URL <https://www.sciencedirect.com/science/article/pii/S0893608005801315>.

[22] Qianxiao Li, Ting Lin, and Zuowei Shen. Deep learning via dynamical systems: An approximation perspective. *arXiv preprint arXiv:1912.10382*, 2019.

[23] Yuying Liu, J. Nathan Kutz, and Steven L. Brunton. Hierarchical Deep Learning of Multiscale Differential Equation Time-Steppers. *arXiv e-prints*, art. arXiv:2008.09768, August 2020.

[24] Yuying Liu, J Nathan Kutz, and Steven L Brunton. Hierarchical deep learning of multiscale differential equation time-steppers. *arXiv preprint arXiv:2008.09768*, 2020.

[25] Lu Lu, Raphael Pestourie, Wenjie Yao, Zhicheng Wang, Francesc Verdugo, and Steven G Johnson. Physics-informed neural networks with hard constraints for inverse design. *arXiv preprint arXiv:2102.04626*, 2021.

[26] Yiping Lu, Aoxiao Zhong, Quanzheng Li, and Bin Dong. Beyond finite layer neural networks: Bridging deep architectures and numerical differential equations. In *International Conference on Machine Learning*, pages 3276–3285. PMLR, 2018.

[27] Dirk M. Luchtenburg, Steven L. Brunton, and Clarence W. Rowley. Long-time uncertainty propagation using generalized polynomial chaos and flow map composition. *Journal of Computational Physics*, 274:783–802, 2014. ISSN 0021-9991. doi: <https://doi.org/10.1016/j.jcp.2014.06.029>. URL <https://www.sciencedirect.com/science/article/pii/S0021999114004367>.

[28] D.P. Mandic, J.A. Chambers, and M.M. Bozic. On global asymptotic stability of fully connected recurrent neural networks. In *2000 IEEE International Conference on Acoustics, Speech, and Signal Processing. Proceedings (Cat. No.00CH37100)*, volume 6, pages 3406–3409 vol.6, 2000. doi: 10.1109/ICASSP.2000.860132.

[29] Stefano Massaroli, Michael Poli, Jinkyoo Park, Atsushi Yamashita, and Hajime Asama. Dissecting neural odes. *arXiv preprint arXiv:2002.08071*, 2020.

[30] K. Mathia and R. Saeks. Solving nonlinear equations using recurrent neural networks. In *World Congress on Neural Networks*, 1995.

[31] Federico Milano. *Power system modelling and scripting*. Springer Science & Business Media, 2010.

[32] Michele Milano and Petros Koumoutsakos. Neural network modeling for near wall turbulent flow. *Journal of Computational Physics*, 182(1):1–26, 2002. ISSN 0021-9991. doi: <https://doi.org/10.1006/jcph.2002.7146>. URL <https://www.sciencedirect.com/science/article/pii/S0021999102971469>.

[33] John Miller and Moritz Hardt. Stable recurrent models. *arXiv preprint arXiv:1805.10369*, 2018.

[34] George S. Misyris, Andreas Venzke, and Spyros Chatzivasileiadis. Physics-informed neural networks for power systems. In *2020 IEEE Power Energy Society General Meeting (PESGM)*, pages 1–5, 2020. doi: 10.1109/PESGM41954.2020.9282004.

[35] Mohamad Mostafa, Werner G. Teich, and Jürgen Lindner. Global vs. local stability of recurrent neural networks as vector equalizer. In *2011 5th International Conference on Signal Processing and Communication Systems (ICSPCS)*, pages 1–5, 2011. doi: 10.1109/ICSPCS.2011.6140866.

[36] J. M. Ortega and W. C. Rheinboldt. *Iterative Solution of Nonlinear Equations in Several Variables*. Society for Industrial and Applied Mathematics, 2000. doi: 10.1137/1.9780898719468. URL <https://pubs.siam.org/doi/abs/10.1137/1.9780898719468>.

[37] Shaowu Pan and Karthik Duraisamy. Long-time predictive modeling of nonlinear dynamical systems using neural networks. *Complexity*, 2018, 2018.

[38] Guofei Pang, Lu Lu, and George Em Karniadakis. fpinns: Fractional physics-informed neural networks. *SIAM Journal on Scientific Computing*, 41(4):A2603–A2626, 2019.

[39] Adam Paszke, Sam Gross, Francisco Massa, Adam Lerer, James Bradbury, Gregory Chanan, Trevor Killeen, Zeming Lin, Natalia Gimelshein, Luca Antiga, Alban Desmaison, Andreas Kopf, Edward Yang, Zachary DeVito, Martin Raison, Alykhan Tejani, Sasank Chilamkurthy, Benoit Steiner, Lu Fang, Junjie Bai, and Soumith Chintala. Pytorch: An imperative style, high-performance deep learning library. In *Advances in Neural Information Processing Systems 32*, pages 8024–8035. Curran Associates, Inc., 2019. URL <http://papers.neurips.cc/paper/9015-pytorch-an-imperative-style-high-performance-deep-learning-library.pdf>.

[40] Vittorino Pata. *Fixed point theorems and applications*, volume 116. Springer, 2019.

[41] Michael Poli, Stefano Massaroli, Junyoung Park, Atsushi Yamashita, Hajime Asama, and Jinkyoo Park. Graph neural ordinary differential equations. *arXiv preprint arXiv:1911.07532*, 2019.

[42] Tong Qin, Kailiang Wu, and Dongbin Xiu. Data driven governing equations approximation using deep neural networks. *Journal of Computational Physics*, 395:620–635, 2019. ISSN 0021-9991. doi: <https://doi.org/10.1016/j.jcp.2019.06.042>. URL <https://www.sciencedirect.com/science/article/pii/S0021999119304504>.

[43] M. Raissi, P. Perdikaris, and G.E. Karniadakis. Physics-informed neural networks: A deep learning framework for solving forward and inverse problems involving nonlinear partial differential equations. *Journal of Computational Physics*, 378:686–707, 2019. ISSN 0021-9991. doi: <https://doi.org/10.1016/j.jcp.2018.10.045>. URL <https://www.sciencedirect.com/science/article/pii/S0021999118307125>.

[44] Max Revay and Ian Manchester. Contracting implicit recurrent neural networks: Stable models with improved trainability. In Alexandre M. Bayen, Ali Jadbabaie, George Pappas, Pablo A. Parrilo, Benjamin Recht, Claire Tomlin, and Melanie Zeilinger, editors, *Proceedings of the 2nd Conference on Learning for Dynamics and Control*, volume 120 of *Proceedings of Machine Learning Research*, pages 393–403, The Cloud, 10–11 Jun 2020. PMLR. URL <http://proceedings.mlr.press/v120/revay20a.html>.

[45] Manuel A Roehrl, Thomas A Runkler, Veronika Brandstetter, Michel Tokic, and Stefan Obermayer. Modeling system dynamics with physics-informed neural networks based on lagrangian mechanics. *arXiv preprint arXiv:2005.14617*, 2020.

[46] Yeonjong Shin, Jerome Darbon, and George Em Karniadakis. On the convergence and generalization of physics informed neural networks. *arXiv preprint arXiv:2004.01806*, 2020.

[47] Patrice Y Simard, Mary B Ottaway, and Dana H Ballard. Fixed point analysis for recurrent networks. In *NIPS*, pages 149–159, 1988.

[48] J.E. Steck. Convergence of recurrent networks as contraction mappings. In *[Proceedings 1992] IJCNN International Joint Conference on Neural Networks*, volume 3, pages 462–467 vol.3, 1992. doi: 10.1109/IJCNN.1992.227131.

[49] Gilbert Strang. *Linear algebra and learning from data*. Wellesley-Cambridge Press Cambridge, 2019.

- [50] Yury Tiumentsev and Mikhail Egorchev. *Neural Network Modeling and Identification of Dynamical Systems*. Academic Press, 2019.
- [51] Belinda Tzen and Maxim Raginsky. Neural stochastic differential equations: Deep latent gaussian models in the diffusion limit. *arXiv preprint arXiv:1905.09883*, 2019.
- [52] Jeremy G. VanAntwerp and Richard D. Braatz. A tutorial on linear and bilinear matrix inequalities. *Journal of Process Control*, 10(4):363–385, 2000. ISSN 0959-1524. doi: [https://doi.org/10.1016/S0959-1524\(99\)00056-6](https://doi.org/10.1016/S0959-1524(99)00056-6). URL <https://www.sciencedirect.com/science/article/pii/S0959152499000566>.
- [53] Zhang Yi. *Convergence analysis of recurrent neural networks*, volume 13. Springer Science & Business Media, 2013.
- [54] Lexing Ying and Emmanuel J Candes. The phase flow method. *Journal of Computational Physics*, 220(1):184–215, 2006.
- [55] Yong Yu, Xiaosheng Si, Changhua Hu, and Jianxun Zhang. A review of recurrent neural networks: Lstm cells and network architectures. *Neural Computation*, 31(7):1235–1270, 2019. doi: 10.1162/neco_a_01199.
- [56] Tianjun Zhang, Zhewei Yao, Amir Gholami, Kurt Keutzer, Joseph Gonzalez, George Biros, and Michael Mahoney. Anodev2: A coupled neural ode evolution framework. *arXiv preprint arXiv:1906.04596*, 2019.

A Derivation of conditions for contraction of Newton's method

By simple application of the Mean Value Theorem [36], a function will necessarily contract if its gradient is everywhere less than 1. In this paper, we are concerned with showing that Newton's method in particular will contract. In the scalar case, Newton's method may be stated simply as $g(x) = x - f(x)/f'(x)$. To ensure the gradient of $g(x)$ is less than 1, we take its derivative, using the quotient rule:

$$\frac{d}{dx}g(x) = 1 - \frac{f'(x)f'(x) - f(x)f''(x)}{f'(x)^2} \quad (22a)$$

$$= \frac{f(x)f''(x)}{f'(x)^2}. \quad (22b)$$

For example, Newton's method will always contract when solving $f(x) = x^2$, since $g'(x) = 2x^2/(4x^2) = 1/2 < 1$. We now extend to the n -dimensional case. Using our previous notation of $\mathbf{K} \triangleq \mathbf{K}_t(\mathbf{k}_2)$ and $\mathbf{J} \triangleq \mathbf{J}_t(\mathbf{k}_2)$, Newton's method is defined in (8) via $\mathbf{G}(\mathbf{k}_2) = \mathbf{k}_2 - \mathbf{J}^{-1}\mathbf{K}$. Taking the multivariable derivative of $\mathbf{G}(\mathbf{k})$ with respect to \mathbf{k} , via product rule, yields

$$\frac{\partial \mathbf{G}(\mathbf{k}_2)}{\partial \mathbf{k}_2} = \mathbf{I} - \left(\mathbf{J}^{-1} \frac{\partial \mathbf{K}}{\partial \mathbf{k}_2} + \frac{\partial}{\partial \mathbf{k}_2} (\mathbf{J}^{-1}) \mathbf{K} \right) \quad (23a)$$

$$= - \frac{\partial}{\partial \mathbf{k}_2} (\mathbf{J}^{-1}) \mathbf{K} \quad (23b)$$

$$= - \left[\begin{array}{cccc} (\frac{\partial}{\partial \mathbf{k}_{21}} \mathbf{J}^{-1}) \mathbf{K} & (\frac{\partial}{\partial \mathbf{k}_{22}} \mathbf{J}^{-1}) \mathbf{K} & \cdots & (\frac{\partial}{\partial \mathbf{k}_{2n}} \mathbf{J}^{-1}) \mathbf{K} \end{array} \right], \quad (23c)$$

since $\mathbf{J} = \partial \mathbf{K} / \partial \mathbf{k}_2$, and where the scalar \mathbf{k}_{2i} is the i^{th} element of \mathbf{k} . We now apply the matrix derivative law [49] which simplifies the expression $\partial \mathbf{A}(x)^{-1} / \partial x = -\mathbf{A}(x)^{-1} (\partial \mathbf{A}(x) / \partial x) \mathbf{A}(x)^{-1}$. Applying this to (23c) yields

$$\frac{\partial \mathbf{G}(\mathbf{k}_2)}{\partial \mathbf{k}_2} = \mathbf{J}^{-1} \left[\begin{array}{cccc} (\frac{\partial}{\partial \mathbf{k}_{21}} \mathbf{J}) \mathbf{J}^{-1} \mathbf{K} & (\frac{\partial}{\partial \mathbf{k}_{22}} \mathbf{J}) \mathbf{J}^{-1} \mathbf{K} & \cdots & (\frac{\partial}{\partial \mathbf{k}_{2n}} \mathbf{J}) \mathbf{J}^{-1} \mathbf{K} \end{array} \right], \quad (24)$$

which is the matrix in (9). If, in some region \mathcal{K} , the singular values of this matrix are everywhere less than 1, then $\mathbf{G}(\mathbf{k}_2)$ must satisfy (2) and will therefore contract.

B Optimal projection via QR decomposition of selected training data

Convergence of the constrained training routine is greatly aided by properly initializing the NN weight matrices. To initialize these weights, an obvious choice is to train an associated unconstrained network and then use the resulting weights to initialize the constrained training routine. In practice, though, directly initializing with an unconstrained solution leads to a very poor initial guess after the projections have been applied. This is partly due to the fact that the (highly tractable) objective function in (20) is totally agnostic to the data which is flowing through the NN. Accordingly, to effectively initialize the constrained training routine, we optimize over the unconstrained problem, and then we “optimally project” the unconstrained solutions into the constrained space by updating the objective function in (20). To build the new objective, we concatenate all data vectors \mathbf{x} flowing through a NN layer (12) into a data matrix $\mathbf{X} = [\mathbf{x}_1, \dots, \mathbf{x}_d]$, where d can be generally very large. We then define a new objective function via $\mathcal{L} = \|(\hat{\mathbf{W}}_i - \mathbf{W}_i)\mathbf{X}\|_F^2$. Defining $\mathbf{B} \triangleq \mathbf{W}_i \mathbf{X}$, a more optimal projection can be written as

$$\min_{\hat{\mathbf{W}}_i} \|\hat{\mathbf{W}}_i \mathbf{X} - \mathbf{B}\|_F^2, \quad \text{s.t. (18) or (19).} \quad (25)$$

Due to the potentially massive size of \mathbf{X} and \mathbf{B} , solving (25) directly is very expensive; accordingly, we precondition the problem to alleviate the computational burden. By properly flattening $\mathcal{F}\{\cdot\}$ and transforming $\mathcal{T}\{\cdot\}$ the matrix quantities in (25) via $\mathcal{T}\{\mathbf{X}\} \rightarrow \mathbf{A} \in \mathbb{R}^{nd \times n^2}$, $\mathcal{F}\{\mathbf{B}\} \rightarrow \mathbf{b} \in \mathbb{R}^{nd \times 1}$, and $\mathcal{F}\{\hat{\mathbf{W}}_i\} \rightarrow \mathbf{y} \in \mathbb{R}^{n^2 \times 1}$, the loss function in (25) can be exactly represented as the overdetermined least squares loss function $\|\mathbf{A}\mathbf{y} - \mathbf{b}\|_2^2$, where \mathbf{A} is “tall and skinny”, and where \mathbf{y} is still suitably constrained by (18) or (19). Overdetermined systems of linear equations can be effectively solved via QR factorization of the matrix \mathbf{A} ; applying this procedure directly to (25), however, will yield an infeasible solution. By the following Lemma, though, the overdetermined system can be transformed into an exactly equivalent system with an equal number of equations and unknowns.

Lemma 3. Factor $\mathbf{A} = \mathbf{QR}$ with a “reduced” QR factorization. The optimal solution of (25) $\hat{\mathbf{W}}_i^*$ coincides with the optimal solution $\mathbf{y}^* \leftarrow \mathcal{F}\{\hat{\mathbf{W}}_i^*\}$ of the following system of n^2 equations/unknowns:

$$\min_{\mathbf{y}} \|\mathbf{R}\mathbf{y} - \mathbf{Q}^T \mathbf{b}\|_2^2, \quad \text{s.t. (18) or (19).} \quad (26)$$

Proof. Assume the QR factorization is “full”: $\mathbf{A} = \mathbf{Q}_f \mathbf{R}_f$. Thus, $\|\mathbf{v}\|_2 = \|\mathbf{Q}_f^T \mathbf{v}\|_2, \forall \mathbf{v}$, and therefore,

$$\|\mathbf{A}\mathbf{y} - \mathbf{b}\|_2^2 = \|\mathbf{Q}_f \mathbf{R}_f \mathbf{y} - \mathbf{b}\|_2^2 = \|\mathbf{R}_f \mathbf{y} - \mathbf{Q}_f^T \mathbf{b}\|_2^2. \quad (27)$$

Since the loss function has not changed in value, the associated constrained solution of $\min\{\|\mathbf{R}_f \mathbf{y} - \mathbf{Q}_f^T \mathbf{b}\|_2^2\}$ will not change. Next, since $\mathbf{R}_f = [\mathbf{R}^T \mid \mathbf{0}^T]^T$, the value of the decision variable \mathbf{y} has no influence over the bottom $n(d - n)$ equations, and an equivalent loss function can be written as $\mathcal{L}_1 = \|\mathbf{R}\mathbf{y} - \mathbf{Q}^T \mathbf{b}\|_2^2 + \|\mathbf{Q}_a^T \mathbf{b}\|_2^2$, where $\mathbf{Q}_f = [\mathbf{Q} \mid \mathbf{Q}_a]$. Thus, the constrained minimizer of \mathcal{L}_1 from the RHS of (27) will be exactly equal to the constrained minimizer of $\mathcal{L}_2 = \|\mathbf{R}\mathbf{y} - \mathbf{Q}^T \mathbf{b}\|_2^2$. Since $\|\mathbf{A}\mathbf{y} - \mathbf{b}\|_2^2 \triangleq \|\hat{\mathbf{W}}_i \mathbf{X} - \mathbf{B}\|_F^2$, the proposition is proved. \square

The computational expense associated with solving (20) and (26) are now equal. However, computing the reduced QR factorization of \mathbf{A} (i.e., \mathbf{X}) is very expensive and cannot be realistically added into a training routine. Thus, we intend for (26) to be a one-time procedure which “optimally” maps an unconstrained weighting matrix into a constrained space. We use this exact procedure when collecting the test results associated with this paper.

C Numerical test results

In this section, we present results and analysis associated with the Hopf bifurcation system and the Kundur electrical power system. For both systems, we train a constrained NN (i.e., CoNNS) on Newton step data in order to model time domain trajectories. For bench-marking purposes, we also train an equivalent unconstrained NN.

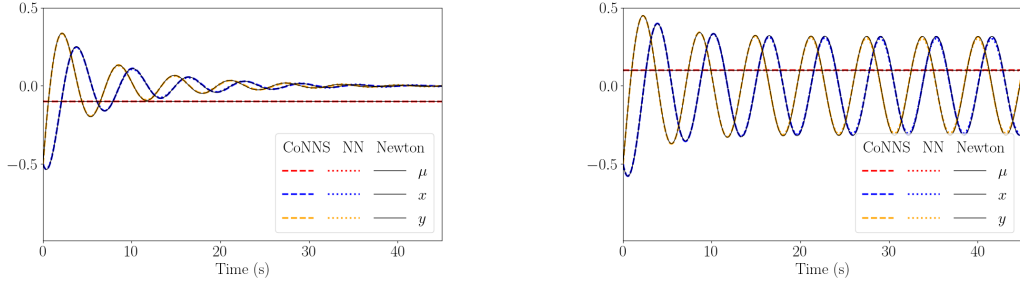
C.1 Hopf bifurcation

The system of equations associated with the Hopf bifurcation has a total of three states: μ , x and y (see Section 5). Accordingly, the size of the NN used to model the cubic oscillator was expanded by an extra ten nodes per layer in order to model the Hopf bifurcation system. The resulting constrained NN performed very well on unseen test data, as shown in Fig. 4. Panel (a) shows a set of initial conditions which converge to an oscillatory limit cycle; panel (b) shows a set of initial conditions which converge to a fixed point. Both panels also show the performance of an unconstrained NN (trained to an equal value of objective loss). Clearly, for the given size of the NN, both models appear to perform very well. Furthermore, when the value of μ is close to 0 (which represents the boundary between limit cycle and fixed point convergence), both models are still able to track the true system trajectories to a high degree of accuracy. We show this in Fig. 5, where we simulated the performance of the two models against test data for $\mu = +0.01$ (left panel) and $\mu = -0.01$ (right panel).

To compare performances more thoroughly, we evaluated the performance of the resulting models by testing them on 50 trajectories stemming from the same distribution on x , y , and μ as in the training set. The results are shown in Table 2. Across all three states, the average test error associated with the constrained NN (i.e., CoNNS) is approximately 20% lower than the test error associated with the unconstrained NN. CoNNS does exhibit slightly higher worst-case error for two of the states; however, its overall performance on unseen test data is superior. In Fig. 6, we show the singular values associated with both NNs.

C.2 Kundur system

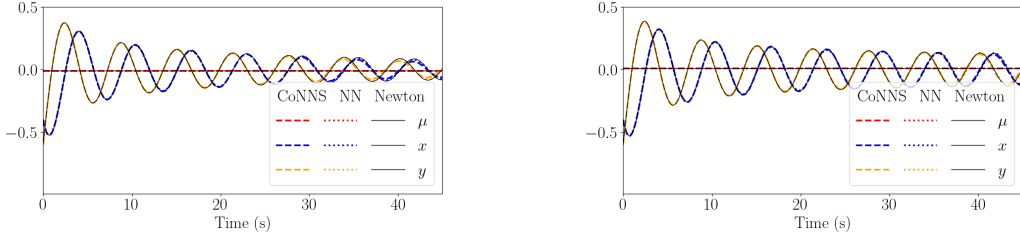
The dynamics of the 10-state Kundur system live in a much higher dimension than both the cubic oscillator and the Hopf bifurcation, so we increased the size of the NN model to 100 nodes per layer with a total of 4 hidden layers. In order to perturb this system in a physically meaningful way, we simulated the effects randomly initializing all of the voltages angle (δ_i) variables in the network;



(a) Hopf Bifurcation (Fixed Point Convergence)

(b) Hopf Bifurcation (Limit Cycle Convergence)

Figure 4: Hopf bifurcation trajectories simulated with Newton, CoNNS and an unconstrained NN. In the left panel, $\mu = -0.1$, so trajectories eventually decay to a fixed point. In the right panel, $\mu = +0.1$, so trajectories converge to a limit cycle.



(a) Hopf Bifurcation (Fixed Point Convergence)

(b) Hopf Bifurcation (Limit Cycle Convergence)

Figure 5: Hopf bifurcation trajectories simulated with Newton, CoNNS and an unconstrained NN. In the left panel, $\mu = -0.01$, so trajectories eventually decay to a fixed point. In the right panel, $\mu = +0.01$, so trajectories converge to a limit cycle. Both NNs, however, are able to capture the high degree of sensitivity that the system has to the initial value of μ .

Table 2: Training and test error associated with the Hopf bifurcation system, computed as the mean, standard deviation, and maximum value of the 2-norm on the approximation error across a trajectory. The number of iterations is the cumulative count of passes through CoNNS or the unconstrained NN.

Hopf bifurcation (constrained)					
Metric	Data	$\ \mu - \hat{\mu}\ _2$	$\ x - \hat{x}\ _2$	$\ y - \hat{y}\ _2$	iterations
mean	Training	0.03047	0.19963	0.20310	28944
sd	Training	0.02103	0.20740	0.20627	1341
max	Training	0.10926	1.40503	1.40369	30605
mean	Test	0.02821	0.19543	0.19447	29180
sd	Test	0.02686	0.14594	0.14626	1110
max	Test	0.15977	0.78966	0.78909	32027

Hopf bifurcation (unconstrained)					
Metric	Data	$\ \mu - \hat{\mu}\ _2$	$\ x - \hat{x}\ _2$	$\ y - \hat{y}\ _2$	iterations
mean	Training	0.03032	0.24344	0.23416	52447
sd	Training	0.02081	0.15492	0.15579	9435
max	Training	0.13449	1.10668	1.09103	79158
mean	Test	0.03574	0.25662	0.24150	51969
sd	Test	0.03352	0.12216	0.11997	9111
max	Test	0.21137	0.69644	0.68634	79512

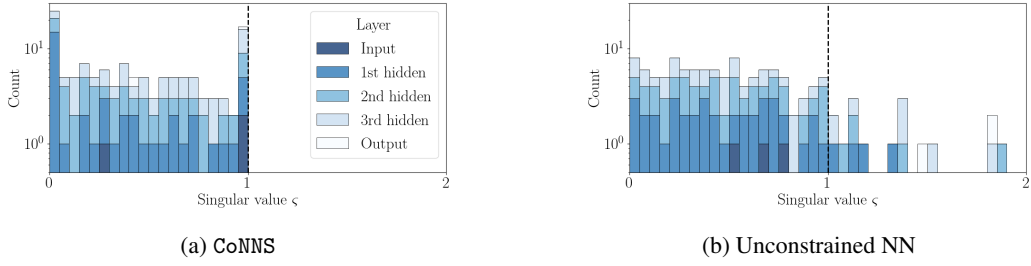


Figure 6: Shown are the singular values of the NN weighting matrices associated with the Hopf bifurcation system. In the case of CoNNS, they are all upper bounded by 1.

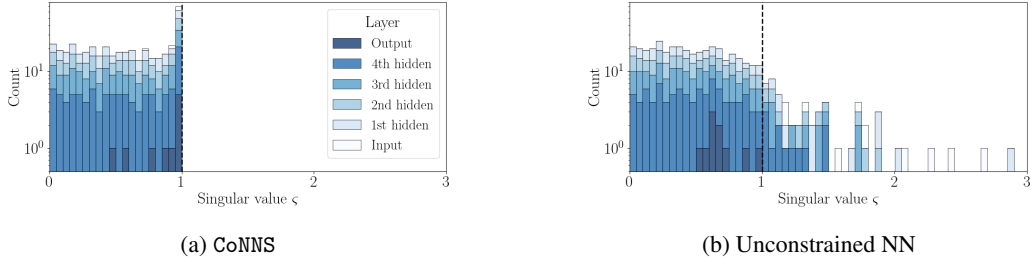


Figure 7: Shown are the singular values of the NN weighting matrices associated with the Kundur system. In the case of CoNNS, they are all upper bounded by 1. Notably, all of the singular values of the input layer are greater than 1 in the unconstrained system.

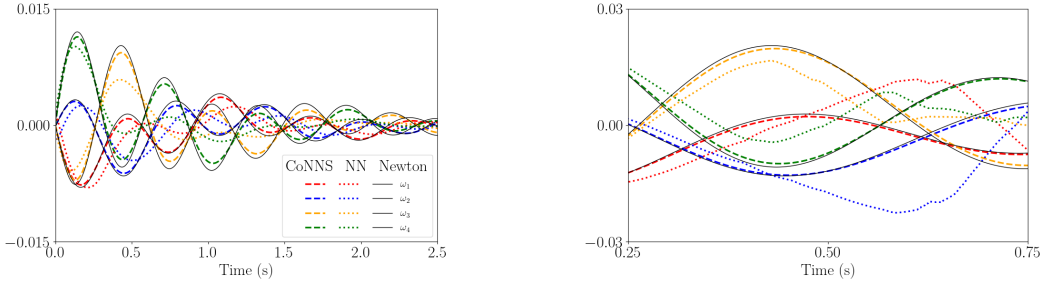
see [20] for a circuit diagram of this system. We simulated 40 system trajectories, each with a time step of $\Delta t = 0.001$ s, for a total of 2.5 seconds.

We trained both CoNNS and an unconstrained NN to an equal value of objective loss ($\mathcal{L} \approx 10^{-6}$). The singular values of both networks are shown in Fig. 7. Notably, all of the singular values of the input layer are larger than unity in the unconstrained system, and the six overall largest singular values are larger than two. We evaluated the performance of the resulting models by testing them on 40 trajectories of test data. In testing, the unconstrained NN would take many hundreds of iterations to converge to a fixed point (and thus, hundreds of thousands of iterations for a single simulation). Accordingly, we softened the convergence criteria down to $\|\Delta \mathbf{x}\|_\infty < 10^{-4}$, and we lowered the standard deviation used to sample the testing data (i.e., perturbation of initial conditions) by a factor of two; this lead to much more reasonable convergence speeds for the unconstrained NN. Finally, we added a maximum iteration threshold (500) for each fixed point, because the unconstrained network appeared to exhibit divergent behaviour for some initial conditions. In the left panel of Fig. 7, we plot Kundur system generator speed (i.e., ω_i) trajectories associated with these modifications. Clearly, CoNNS shows a superior ability to track the true trajectories. In the right panel of this figure, we show the performance of the NNs when the testing data is sampled from the original distributions (and for necessity, convergence criteria is softened even further to $\|\Delta \mathbf{x}\|_\infty < 10^{-3}$). In this case, the unconstrained NN shows sharp (i.e., non-smooth) incoherent trajectories which are very poor predictors of the true underlying signals. In Table 3, we offer direct comparisons between CoNNS and the unconstrained NN across the full test set; once again, CoNNS shows better predictive performance, and it requires a much smaller number of iterations.

D Universal Approximation Proof

On the metric space (\mathcal{X}, d) , and we define $\mathcal{C}(\mathcal{X})$ as the vector space of all contracting functions.

Proof of Theorem 3. An unconstrained feedforward NN with ReLU activation functions, characterized by the mapping $\Phi_u : \mathbb{R}^n \rightarrow \mathbb{R}^n$, is necessarily dense in the space of continuous functions [21].



(a) Kundur System (Test Trajectory)

(b) Test Trajectory with Larger Perturbation

Figure 8: In the left panel, we show generator speed test trajectories associated with the Kundur system as simulated by Newton, CoNNs, and the unconstrained NN. The right panel showcases the extremely poor predictive behaviour of the unconstrained NN when the initial conditions are perturbed by a larger margin.

Table 3: Test error associated with the Kundur system, computed as the mean, standard deviation, and maximum value of the 2-norm on the approximation error across a trajectory. The number of iterations is the cumulative count of passes through CoNNs or the unconstrained NN. Test data was sampled using a distribution with a smaller standard deviation than the distribution used to sample the training data (see text), so the training data error is not included in this table.

Metric	Data	Kundur (constrained)		Kundur (unconstrained)	
		$\ \mathbf{x} - \hat{\mathbf{x}}\ _2$	iterations	$\ \mathbf{x} - \hat{\mathbf{x}}\ _2$	iterations
mean	Test	0.02349	31631	0.12250	107522
sd	Test	0.01027	12011	0.06071	60464
max	Test	0.04691	58632	0.25038	290641

Since any contracting function is, by necessity, uniformly continuous [36], $\mathcal{C}(\mathcal{X})$ is a proper subset of the space of continuous functions. Therefore, an unconstrained (i.e., standard) feedforward NN with ReLU activation functions is necessarily dense in $\mathcal{C}(\mathcal{X})$. Since it is dense in $\mathcal{C}(\mathcal{X})$, we assume it can be, and is, trained to satisfy the contraction mapping definition, i.e., Definition 1, $\forall \mathbb{R}^n$.

While Φ_u does contract, it does not necessarily satisfy (14), since individual layers may not necessarily contract. Next, we assume that there exists some constrained, feedforward NN $\Phi_c : \mathbb{R}^n \rightarrow \mathbb{R}^n$, also equipped with ReLU activation functions, and which does satisfy (14). Clearly, condition (14) directly implies contraction, but condition (14) does not limit the output range of Φ_c to be less than that of Φ_u . For a given input domain, Φ_u and Φ_c can thus both reach the same range of outputs, assuming Φ_c is given a sufficiently large parameter space (i.e., depth), and it can therefore provide mapping which is identical (in a dense sense) to that of Φ_u . Since Φ_u is dense in $\mathcal{C}(\mathcal{X})$, and since Φ_c can provide identical input-output mapping, by syllogism, Φ_c is therefore also dense in $\mathcal{C}(\mathcal{X})$. Accordingly, it can provide universal approximation of any contracting function which satisfies (2). \square